A&A 412, 587–595 (2003)
DOI: 10.1051/0004-6361:20031462

Astronomy & Astrophysics

Dielectronic recombination data for dynamic finite-density plasmas

II. The oxygen isoelectronic sequence

O. Zatsarinny[1], T. W. Gorczyca[1], K. T. Korista[1], N. R. Badnell[2], and D. W. Savin[3]

[1] Department of Physics, Western Michigan University, Kalamazoo, MI 49008, USA
e-mail: oleg.zatsarinny@wmich.edu; [gorczyca; korista]@physics.wmich.edu
[2] Department of Physics, University of Strathclyde, Glasgow, G4 0NG, UK
[3] Columbia Astrophysics Laboratory, Columbia University, New York, 10027, USA
e-mail: savin@astro.columbia.edu

Received 19 May 2003 / Accepted 18 September 2003

Abstract. Dielectronic recombination (DR) and radiative recombination (RR) data for oxygen-like ions forming fluorine-like ions have been calculated as part of the assembly of a level-resolved DR and RR database necessary for modelling of dynamic finite-density plasmas (Badnell et al. 2003). Total DR and RR rate coefficients for F^{+} to Zn^{22+} are presented and the results discussed. By comparison between perturbative and R-matrix results, we find that RR/DR interference effects are negligible even for the lowest-charged F^{+} member. We also find that the $2 \rightarrow 2$ low-temperature DR (no change in the principal quantum number of the core electrons) does not scale smoothly with nuclear charge Z due to resonances straddling the ionization limit, thereby making explicit calculations for each ion necessary. These RR and DR data are suitable for modelling of solar and cosmic plasmas under conditions of collisional ionization equilibrium, photoionization equilibrium, and non-equilibrium ionization.

Key words. atomic data – atomic processes – plasmas

1. Introduction

The measurement of chemical abundances throughout cosmic space and time is a major goal in astrophysics. At great distances and look-back times, quasar broad emission line regions, the intergalactic medium, and birthing and rapidly evolving starburst galaxies offer astronomers the opportunity to study the chemical evolution of the universe. The local universe offers spatially-resolved star forming regions, planetary nebulae, novae, supernovae, and the interstellar medium that yield information concerning the heavy element enrichment by stars in the Milky Way and nearby galaxies, and act as calibrating sources for understanding the high redshift universe.

Most estimates of chemical composition come from the quantitative analysis and interpretation of spectra, frequently of emitting plasmas that are at extremely low density by laboratory standards. Spectral simulations of these plasmas must rely on a vast database of basic atomic and molecular cross sections and transition rates. One of the most important of these processes, and one of the least accurate in the existing astrophysical data base, is dielectronic recombination (DR).

Send offprint requests to: T. W. Gorczyca,
e-mail: thomas.gorczyca@wmich.edu

Our program to generate a reliable level-resolved DR database, necessary for spectroscopic modelling of plasmas in ionization equilibrium and non-equilibrium, has been described by Badnell et al. (2003). The database includes total and final-state, level-resolved results. Calculations are being carried out in intermediate coupling to produce DR data for the isoelectronic sequences of all first and second row elements. In this paper, we describe calculations and results of DR data for oxygen-like ions forming fluorine-like ions. Ions from the oxygen-like isoelectronic sequence are found in photoionized environments, as well as in high temperature collisionally ionized gases.

Although a few theoretical studies of this isoelectronic sequence have been made, there are large differences in the results from different calculations. For example, Savin & Laming (2002) investigated how the relative elemental abundances inferred from the solar upper atmosphere are affected by uncertainties in the total DR rate coefficients used to analyze the spectra. They found that the inferred relative abundances can be up to a factor of 5 smaller or 1.6 larger than those inferred using the currently recommended data from Mazzotta et al. (1998). They also estimated the uncertainty in the high-temperature total DR rate coefficients for oxygen-like ions to be a factor

of ∼3, and concluded that accurate rate coefficients for DR of oxygen-like ions presently have the highest priority among the enormous amount of DR data needed for modelling solar and stellar upper atmospheres.

One of the first calculations of total DR rate coefficients for oxygen-like ions was carried out by Jacobs et al. (1977, 1979, 1980) for Ne, Mg, Si, S, Ca, Fe, and Ni ions using a simple model to describe the DR process. In this model, the autoionization rates are obtained from the threshold values of the partial-wave electron-impact excitation cross sections for the corresponding ions by means of the quantum-defect theory relationship (Seaton 1969) between these values. The excitation cross sections were obtained in the distorted-wave approximation in the LS-coupling scheme, and only dipole 2s–2p, 2p–3s and 2p–3d transitions were included. In addition, radiative decay of autoionizing states was approximated as the ionic core radiative decay rate. Comparison with the latest data shows that this simplified model gives rather accurate high-temperature total DR rate coefficients for Ne^{2+}, Mg^{4+} and Si^{6+} ions, but underestimates total DR rate coefficients for S^{8+} and Fe^{18+} by a factor of 2.6 at the high-temperature peak in the total DR rate coefficient. These total DR rate coefficients were then fitted by Shull & van Steenberg (1982) and used in their ionization balance calculations.

Roszman (1987) performed more detailed calculations, and presented total DR rate coefficients for the Ar^{10+}, Fe^{18+}, Kr^{28+}, and Mo^{34+} ions. A frozen-core model of the atomic structure with the single-configuration approximation, LS-coupling, and the distorted-wave approximation was used to compute the orbital energies, the radiative transition rates, and the autoionization rates. Roszman included all $2 \rightarrow 2$ (no change in the principal quantum number n_c of the core electrons) and $2 \rightarrow 3$ ($\Delta n_c = 1$ of a core electron) configurations, all dipole-allowed radiative transitions which lead to recombination, and all energetically possible autoionization transitions. The numerical results for low-n contributions were extrapolated to the $n = \infty$ limit, as needed for the computation of the total DR rate coefficients. Roszman also provided an analytic interpolation formula for estimating the total DR rate coefficients for ions with intermediate charge. In addition to the ground state DR, he also presented the total DR rate coefficients from the excited $2s^2 2p^4(^1S,^1D)$ and $2s2p^5(^1P,^3P)$ multiplets. Such data can be useful in modelling dynamic plasmas. At the high-temperature peak in the DR rate coefficient, the data from Roszman differ by about 60% from the Fe^{18+} total DR rate coefficients of Jacobs et al. (1979). This was attributed to the omission of non-dipole transitions in the calculations of Jacobs et al.

Detailed DR computational data, such as singly and doubly excited-state energies, autoionization rates to ground and excited states, radiative decay rates to singly excited states, and DR branching ratios, were presented by Dasgupta & Whitney (1994) for recombination from oxygen-like to fluorine-like Ar, Ti, Fe, and Se ions. These were later extended to Mo^{34+} by Dasgupta & Whitney (1995). The calculations were performed in an intermediate-coupling, single-configuration approximation, where the wavefunctions and energies of bound and autoionizing states were calculated using the Hartree-Fock method with relativistic corrections, using the code of Cowan (1981). The detailed state-specific DR data presented by Dasgupta & Whitney are required for modelling the effect of DR on excited-state populations, for example, in order to calculate the X-ray laser gain under certain plasma conditions. A comparison of total DR rate coefficients for Ar and Fe ions showed dramatic differences (up to a factor of 2.6 at the maximum of the total DR rate coefficient) from the results of Roszman (1987). Such large differences were attributed to Roszman's use of an LS-coupled scheme, whereas Dasgupta & Whitney used an intermediate coupling scheme.

The available theoretical results were fitted by Mazzotta et al. (1998), and tabulated in their study of the ionization equilibrium for a range of atoms and ions. For Ar through Ni, they used the results of Dasgupta & Whitney (1994), and for all other elements, they used the fitting of Shull & van Steenberg (1982) based on the results of Jacobs et al. (1977, 1979, 1980). Note, that those available results used by Mazzotta et al. (1998) apply only at $kT > 1$ eV.

The only existing experimental DR measurements for oxygen-like ions are for Fe^{18+}, done by Savin et al. (1999) for $2 \rightarrow 2$ DR and by Savin et al. (2002a) for $2 \rightarrow 3$ DR using the heavy-ion Test Storage Ring in Heidelberg, Germany. The cooler electrons employed in this technique allowed for the resolution of resonances associated with $2 \rightarrow 2$ and $2 \rightarrow 3$ excitations and some resolution of fine-structure components. Significant discrepancies were found between experimentally derived total DR rate coefficients and previously published theoretical results. Those calculated total DR rate coefficients differed by factors of 2–10 from the experimental ones. Thus the measurements called into question all previous theoretical total DR rate coefficients (especially the $2 \rightarrow 2$ data) used for ionization balance calculations of cosmic plasmas. In the work of Savin et al. (1999, 2002a), new theoretical calculations were also carried out using multiconfiguration Dirac-Fock (MCDF) and intermediate-coupling multiconfiguration Breit-Pauli (MCBP) approaches. These new theoretical results agree with the measured resonance strengths and total DR rate coefficients to within 30% for $2 \rightarrow 2$ DR and typically 20% for the $2 \rightarrow 3$ DR.

As the result of these measurements a new series of state-of-the-art calculations have been carried out. Chen (2002) has carried out MCDF calculations for four members of the oxygen-like sequence: Mg^{4+}, Si^{6+}, S^{8+}, and Fe^{18+}. Gu (2003a,b) has used the Flexible Atomic Code (FAC) to calculate DR data for oygenlike ions of Mg, Si, S, Ar, Ca, Fe, and Ni.

In this paper, we use the intermediate-coupling MCBP method, in the isolated resonance approximation, to compute partial and total DR rate coefficients for all oxygen-like ions from F^+ to Zn^{22+}. This is similar to the method used in Savin et al. (2002a). In order to investigate the effects of interference between DR and radiative recombination (RR), we also performed R-matrix calculations of unified DR+RR for the cases of F^+ and Ne^{2+} ions. The overall effect of interference between the DR and the background RR for total rate coefficients was found to be quite small. The total rate coefficients detailed here cover a wide range of temperatures and ionic species, and are expected to be broadly accurate in most respects. We note, however, that storage ring results have

demonstrated that all theoretical methods (e.g., MCBP, MCDF, and R-matrix) are not able to reproduce reliably the DR resonance strengths and energies of L-shell ions for relative collision energies $\lesssim$2–3 eV (e.g., Savin et al. 1999, 2002b; Schippers et al. 2001). For reliable total DR rate coefficients at plasma temperatures where these resonances play a significant role, these theoretical results need to be supplemented with storage ring measurements of the relevant resonances. Nevertheless, we have ascertained, through a careful study for the present oxygen-like sequence, that no such low-energy resonances exist at energies close to the temperatures where these ions are predicted to form in either photoionized equilibrium or collisional ionization equilibrium.

The present calculations also attempt to produce final state-resolved DR coefficients, which are important in modelling dense plasmas. Total DR rate coefficients (along with total RR rate coefficients) are presented in compact form using a simple fitting formula. Data are presented for each ion, since the large irregularity in Z-dependence of the total DR rate coefficients at low temperatures makes scaling inaccurate. It is impractical to list all level-resolved rate coefficients in this publication. As previously discussed (Badnell et al. 2003), the present data will form part of an Atomic Data and Analysis Structure (ADAS) dataset comprising the *adf09* files for each ion, detailing the rate coefficients to each LSJ-resolved final state. These data are available through the ADAS project (Summers 1999), and is also made available online at the Oak Ridge Controlled Fusion Atomic Data Center (`http://www-cfadc.phy.ornl.gov/data_and_codes`).

The rest of this paper is organized as follows: in Sect. 2 we give a brief description of the theory used and the details of our calculations for the oxygen-like ions. In Sect. 3 we present the results for the total DR rate coefficients for 22 ions in this sequence. We conclude with a brief summary in Sect. 4.

2. Theory

Details of our calculations have already been described elsewhere (Badnell et al. 2003). Here we outline only the main points. DR calculations were carried out using the code AUTOSTRUCTURE (Badnell 1986; Badnell & Pindzola 1989) which is based on lowest-order perturbation theory, where both the electron–electron and electron–photon interactions are treated to first order. This independent-processes, isolated-resonance approximation is used to calculate configuration-mixed LS and IC energy levels, radiative rates, and autoionization rates, which are then used to compute Lorentzian DR resonance profiles. This enables the generation of final state level-resolved and total DR rate coefficients. We neglect interference between RR and DR, which we will show does not affect the dominant rate coefficients.

The DR process for oxygen-like ions of an arbitrary atom A can be represented, in intermediate coupling, as

$$\mathrm{e}^- + A^{q+}(2\mathrm{s}^2 2\mathrm{p}^4[^3\mathrm{P}_2]) \rightarrow \left\{\begin{array}{l} A^{(q-1)+}(2\mathrm{s}^2 2\mathrm{p}^4[^3\mathrm{P}_{0,1};\ ^1\mathrm{D}_2;\ ^1\mathrm{S}_0]nl) \\ A^{(q-1)+}(2\mathrm{s}2\mathrm{p}^5[^3\mathrm{P}^{\mathrm{o}}_{0,1,2};\ ^1\mathrm{P}^{\mathrm{o}}_1]nl) \\ A^{(q-1)+}(2\mathrm{p}^6[^1\mathrm{S}_0]nl). \end{array}\right\} \rightarrow A^{(q-1)+} + h\nu \quad (1)$$

for $2 \rightarrow 2$ core excitations, where we included all $0 \le l \le 15$ and $n_{\min} \le n \le 1000$ ($n_{\min}$ is the lowest autoionizing state, which varies from $n_{\min} = 4$ for F^+ to $n_{\min} = 6$ for Xe^{46+}). For $2 \rightarrow 3$ core excitations, the DR process can be written as

$$A^{q+}(2\mathrm{s}^2 2\mathrm{p}^4[^3\mathrm{P}_2]) + \mathrm{e}^- \rightarrow \left\{\begin{array}{l} A^{(q-1)+}(2\mathrm{s}^2 2\mathrm{p}^3 3lnl') \\ A^{(q-1)+}(2\mathrm{s}2\mathrm{p}^4 3lnl') \end{array}\right\} \rightarrow A^{(q-1)+} + h\nu\,, \quad (2)$$

where we have included all $0 \le l \le 6$ and $3 \le n \le 1000$ (higher-l DR drops off faster in this case).

A bound orbital basis (1s, 2s, 2p, 3s, 3p, 3d) was generated from a configuration-average Hartree-Fock (Froese Fischer 1991) calculation for the $1s^2 2s^2 2p^4$ configuration to obtain the first three orbitals, followed by a configuration-average, frozen-core HF calculation for the $1s^2 2s^2 2p^3 3l$ states to obtain the additional $n = 3$ orbitals. Then, the corresponding atomic structures for the initial ionic states, the intermediate resonance states, and the final recombined states were obtained by diagonalizing the appropriate Breit-Pauli Hamiltonian. All target states were obtained with full configuration and spin-orbit mixing of configurations indicated in Eqs. (1) and (2). Prior to the final DR calculations, the ionic thresholds were shifted to the known spectroscopic values (`http://physics.nist.gov/cgi-bin/AtData/main_asd`) by a small amount – typically in the range of 1–2 eV for high Z. Distorted wave calculations were then performed to generate the appropriate free εl and bound nl ($n > 3$) orbitals which are attached to each target state to yield the continuum and resonance states, respectively. All of the above orbitals are computed in the absence of any relativistic effects. However, the continuum and resonance states are subsequently recoupled to an intermediate coupling scheme in order to include relativistic effects to lowest order. Also, the DR contribution from $3l3l'$ autoionizing states is considered separately, with full configuration and spin–orbit mixing between these states.

The computed DR data is a sum of Lorentzian profiles and can therefore be convoluted analytically with the experimental energy distribution, in order to compare to measured results, or with a Maxwellian electron distribution, in order to obtain total DR rate coefficients. This represents a huge savings in computational effort over R-matrix calculations since the latter must be performed for an extremely dense energy mesh in order to fully resolve all resonances (Gorczyca et al. 2002; Ramirez & Bautista 2002). The total DR rate coefficients were then fitted as

$$\alpha_{\mathrm{DR}}(T) = T^{-3/2} \sum_i c_i \mathrm{e}^{-E_i/T} \quad (3)$$

in order to facilitate the further application of our data. Here the temperature T and the energy fitting parameter E_i are in units of eV, and the rate coefficient $\alpha_{\mathrm{DR}}(T)$ is in units 10^{-11} cm^3 s^{-1}. Table 1 lists the fitting parameters c_i and E_i for each member of the oxygen-like sequence treated. The fits are accurate to within a maximum difference of 3% for 0.001 eV $< T <$ 100 000 eV. This covers the temperature range over which the ions discussed in this paper are predicted to form in both photoionization equilibrium and collisional ionization equilibrium.

Note that different parameters c_i and E_i in Table 1 reflect different recombination channels in Eqs. (1) and (2): Cols. 2–5 correspond to the $2 \rightarrow 2\ \Delta l = 0$ channels in first line of Eq. (1), Cols. 6 and 7 to the $2 \rightarrow 2\ \Delta l = 1$ channels in the second line of Eq. (1), and Cols. 8 and 9 to the $2 \rightarrow 3$ ($n = 3$) and ($n > 3$) channels in Eq. (2), respectively.

In order to provide total (DR+RR) recombination rate coefficients, Table 1 also contains the fitting coefficients for the RR rate coefficients. These were also obtained using the AUTOSTRUCTURE code with the same target orbitals and in the same approximation as the DR calculations. RR rate coefficients were fitted with the formula of Verner & Ferland (1996)

$$\alpha_{\rm RR}(T) = a\left[\sqrt{T/T_0}\left(1+\sqrt{T/T_0}\right)^{1-b}\left(1+\sqrt{T/T_1}\right)\right]^{-1}, \qquad (4)$$

where the fitting parameters T_0 and T_1 are in units of eV, a is in units of 10^{-11} cm^3 s^{-1}, and b is dimensionless. This form ensures the correct asymptotic behavior of the RR rate coefficients for low and high temperatures: $\alpha_{\rm RR}(T) \propto T^{-1/2}$ at $T \ll T_0, T_1$, and $\alpha_{\rm RR}(T) \propto T^{-3/2}$ at $T \gg T_0, T_1$. The average accuracy of the fitting is better than 4% in the temperature range 10^{-5} eV to 10^{+5} eV (the error is less than 8% for all ions at all temperatures).

AUTOSTRUCTURE is implemented within the ADAS suite of programs as ADAS701. It produces raw autoionization and radiative rates which must be post-processed to obtain the final state level-resolved and total DR rate coefficients. The post-processor ADASDR is used to reorganize the resultant data and also to add in radiative transitions between highly-excited Rydberg states, which are computed hydrogenically. This post-processor outputs directly the *adf09* file necessary for use by ADAS. The *adf09* files generated by our calculations in the IC configuration mixed approximations are available electronically[1]. They provide final state level-resolved DR rate coefficients into final LSJ levels in a manner useful to fusion and astrophysical modelers. Separate files *adf09* are produced for the core excitations $2 \rightarrow 2$, $2 \rightarrow 3$ (capture to $n = 3$), and $2 \rightarrow 3$ (capture to $n > 3$), including final-state level-resolved DR data from both the ground and metastable states.

3. Results

Because of the complexity of the theoretical description for the DR process, it is almost impossible to say a priori which approximations in the calculations are justified and which are not. Laboratory measurements are needed to ensure that even state-of-the-art techniques produce reliable results. Before carrying out the systematic calculations for DR rate coefficients for a whole sequence, we therefore first checked the chosen approximations by comparing to the available experimental data. Figure 1 presents the comparison of our calculations of total DR rate coefficients with results of measurements using the heavy-ion TSR in Heidelberg (Savin et al. 1999, 2002a) for Fe^{18+} to Fe^{17+} recombination. For the $2 \rightarrow 2$ measurements, the cooler electrons employed in this technique had an anisotropic Maxwellian distribution with low perpendicular and parallel

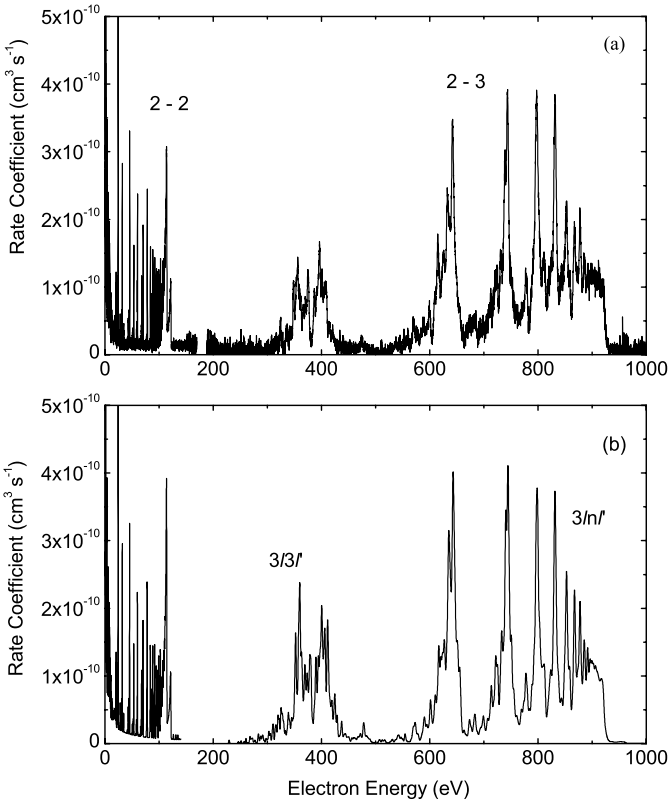

Fig. 1. Fe^{18+} to Fe^{17+} total DR rate coefficients due to $2 \rightarrow 2$ and $2 \rightarrow 3$ core excitations: **a)** TSR experiment (Savin et al. 1999, 2002a); **b)** the present MCBP calculations with the RR contribution added, which is responsible for the upward curve of the background with decreasing energy.

temperatures of $kT_\perp \approx 17$ meV and $kT_\parallel \approx 0.15$ meV, and allow resolution of separated resonances associated with $2 \rightarrow 2$ core excitations. For the $2 \rightarrow 3$ measurements, the effective temperature was $kT_{\rm eff} \approx 1.125$ meV. These measurements therefore allow a very detailed comparison for the DR process. As seen in Fig. 1, our calculations based on the MCBP method in the isolated-resonance approximation reproduce all the main resonances and their intensities fairly well. The most notable discrepancies are for the $3l3l'$ resonances (≈50%). All other resonance intensities agree with experiment to within ±≈30%.

The Maxwellian total DR rate coefficients for Fe^{18+} as a function of electron temperature are compared in Fig. 2 with experimentally derived results and other published theoretical results. Our MCBP total DR rate coefficients agree closely with experimental results within the estimated experimental uncertainty of ≈20%. Also shown in Fig. 2a are the contributions from just the $2 \rightarrow 3$ and $2 \rightarrow 4$ core excitations. This characterizes the importance of the different processes in Eqs. (1) and (2) in the total DR rate coefficient. At low electron temperatures ($kT \approx$ 10–50 eV), where Fe^{18+} is predicted to peak in fractional abundance in an optically thin, photoionized plasma with cosmic abundances (Kallman & Bautista 2001), the main contribution to the total DR rates comes from the $2 \rightarrow 2$ core excitation. In an electron-ionized plasma, the peak in abundance of Fe^{18+} is predicted at $kT \approx 685$ eV (Mazzotta et al. 1998). In this region, the main contribution to the total DR rate

[1] http://www-cfadc.phy.ornl.gov/data_and_codes

Table 1. Fitting coefficients of Eqs. (3) and (4) for dielectronic and radiative recombination of O-like ions forming F-like systems: Cols. 2–5 correspond to $2 \rightarrow 2\ \Delta l = 0$ DR, Cols. 6 and 7 to the $2 \rightarrow 2\ \Delta l = 1$ DR, Col. 8 to the $2 \rightarrow 3$ ($n = 3$) DR, Col. 9 to the $2 \rightarrow 3$ ($n > 0$) DR, and Cols. 10 and 11 to the calculated RR coefficients. The c_i and a are in units of 10^{-11} cm^3 s^{-1}, the E_i, T_0, and T_1 are in eV, and b is dimensionless.

Ion	c_1	c_2	c_3	c_4	c_5	c_6	c_7	c_8	a	b
F^{+}	2.900E−04	2.000E−05	6.800E−04	8.000E−05	9.000E+00	1.600E−03	2.520E+00	7.064E−01	8.782E+00	6.873E−01
Ne^{2+}	4.200E−04	9.100E−04	4.740E−03	8.960E−03	0.000E+00	2.161E+02	8.810E+00	5.734E+00	3.652E+01	7.459E−01
Na^{3+}	1.570E−03	3.390E−03	1.376E−02	1.534E−01	2.314E+00	4.051E+02	5.385E+01	3.934E+01	1.221E+02	7.998E−01
Mg^{4+}	1.594E−01	1.542E−01	2.853E−01	2.656E+00	6.235E+00	6.118E+02	1.407E+02	2.205E+02	2.016E+02	8.176E−01
Al^{5+}	3.620E−02	1.175E−01	2.471E−01	1.539E+00	2.566E+00	5.840E+02	3.456E+02	8.199E+02	2.813E+02	8.265E−01
Si^{6+}	1.020E−03	2.566E−02	1.054E−01	2.255E+00	1.199E+01	1.071E+03	6.868E+02	2.075E+03	3.076E+02	8.252E−01
P^{7+}	2.490E−03	3.135E−01	2.738E+00	5.700E+00	2.092E+01	1.361E+03	1.131E+03	4.255E+03	3.405E+02	8.238E−01
S^{8+}	3.799E−02	8.901E−01	1.640E+00	3.308E+01	2.076E+01	1.535E+03	1.800E+03	8.160E+03	3.300E+02	8.185E−01
Cl^{9+}	6.708E−02	4.497E−01	3.710E+00	8.255E+00	7.385E+01	1.782E+03	2.566E+03	1.278E+04	3.629E+02	8.183E−01
Ar^{10+}	2.570E−02	3.916E−01	4.706E+00	7.879E+01	1.306E+02	1.952E+03	3.585E+03	1.942E+04	3.516E+02	8.120E−01
K^{11+}	2.977E−01	1.821E+00	3.626E+00	1.000E+02	1.385E+02	2.222E+03	4.777E+03	2.810E+04	3.686E+02	8.093E−01
Ca^{12+}	1.771E+00	2.230E+00	6.743E+01	4.402E+01	1.706E+02	2.505E+03	6.231E+03	3.851E+04	3.833E+02	8.070E−01
Sc^{13+}	4.526E−01	1.015E+00	1.168E+01	3.846E+01	1.979E+02	2.769E+03	8.169E+03	4.920E+04	3.906E+02	8.044E−01
Ti^{14+}	1.797E+00	9.051E+00	3.945E+01	2.403E+02	2.725E+02	2.910E+03	1.019E+04	6.092E+04	4.187E+02	8.024E−01
V^{15+}	2.477E+00	1.522E+01	1.118E+02	3.607E+02	3.010E+02	3.194E+03	1.285E+04	7.459E+04	4.320E+02	8.018E−01
Cr^{16+}	1.266E+00	4.808E+00	8.026E+01	3.350E+02	3.432E+02	3.472E+03	1.558E+04	8.844E+04	4.255E+02	7.961E−01
Mn^{17+}	1.473E+00	4.512E+00	3.433E+01	3.120E+02	4.188E+02	3.839E+03	1.879E+04	1.027E+05	4.690E+02	7.993E−01
Fe^{18+}	2.236E+00	1.788E+00	3.074E+00	5.024E+01	5.695E+02	3.896E+03	2.262E+04	1.176E+05	4.010E+02	7.854E−01
Co^{19+}	4.720E−02	1.869E+00	1.174E+01	5.702E+01	3.737E+02	5.585E+03	2.647E+04	1.337E+05	4.597E+02	7.910E−01
Ni^{20+}	2.419E−01	4.723E+00	5.685E+01	6.430E+02	6.825E+02	4.581E+03	3.064E+04	1.511E+05	4.550E+02	7.862E−01
Cu^{21+}	1.556E+00	1.390E+01	7.181E+01	1.169E+03	7.515E+02	5.019E+03	3.668E+04	1.615E+05	5.090E+02	7.915E−01
Zn^{22+}	1.114E+00	2.288E+00	8.787E+01	1.406E+03	7.927E+02	5.470E+03	3.991E+04	1.760E+05	5.066E+02	7.873E−01
Kr^{28+}	3.722E+00	1.308E+02	1.279E+03	4.650E+03	1.250E+03	7.853E+03	8.058E+04	2.602E+05	5.641E+02	7.788E−01
Mo^{34+}	8.138E+00	2.366E+02	8.310E+02	6.402E+03	9.990E+02	2.565E+03	1.260E+05	3.251E+05	6.518E+02	7.754E−01
Cd^{40+}	2.797E+01	1.059E+02	3.565E+02	4.629E+03	1.269E+03	2.961E+03	1.696E+05	3.686E+05	7.145E+02	7.707E−01
Xe^{46+}	9.152E+01	6.568E+02	5.557E+03	3.213E+04	2.516E+03	1.014E+04	1.999E+05	3.895E+05	7.674E+02	7.657E−01
	E_1	E_2	E_3	E_4	E_5	E_6	E_7	E_8	T_0	T_1
F^{+}	3.700E−04	2.080E−03	1.009E−02	1.478E−02	0.000E+00	1.182E+00	2.047E+01	3.345E+01	1.600E−04	4.104E+00
Ne^{2+}	1.730E−03	4.240E−03	1.791E−02	7.318E−02	0.000E+00	2.468E+01	2.654E+01	3.835E+01	1.700E−04	2.121E+01
Na^{3+}	1.070E−03	2.350E−03	2.246E−02	2.079E−01	9.672E+00	2.938E+01	4.772E+01	6.182E+01	9.000E−05	4.914E+01
Mg^{4+}	1.230E−03	7.110E−03	1.303E−01	1.530E+00	1.196E+01	3.396E+01	7.218E+01	8.762E+01	1.100E−04	8.750E+01
Al^{5+}	5.620E−02	1.488E−01	4.623E−01	1.799E+00	8.079E+00	4.283E+01	8.988E+01	1.172E+02	1.400E−04	1.264E+02
Si^{6+}	1.630E−03	1.806E−02	7.632E−02	3.136E−01	6.585E+00	4.146E+01	1.079E+02	1.487E+02	2.400E−04	1.853E+02
P^{7+}	4.489E−02	1.422E−01	5.323E−01	1.632E+00	6.697E+00	4.551E+01	1.274E+02	1.846E+02	3.600E−04	2.520E+02
S^{8+}	6.690E−03	2.135E−02	9.720E−02	6.974E−01	1.125E+01	5.038E+01	1.453E+02	2.226E+02	6.400E−04	3.305E+02
Cl^{9+}	2.038E−02	4.935E−02	3.210E−01	1.623E+00	1.653E+01	5.581E+01	1.661E+02	2.631E+02	8.400E−04	4.001E+02
Ar^{10+}	2.063E−02	6.455E−02	5.363E−01	3.366E+00	3.115E+01	6.223E+01	1.866E+02	3.069E+02	1.340E−03	5.082E+02
K^{11+}	6.880E−03	2.836E−02	1.140E−01	2.800E+00	2.792E+01	6.632E+01	2.074E+02	3.534E+02	1.780E−03	5.968E+02
Ca^{12+}	6.178E−02	1.196E−01	6.601E−01	4.375E+00	2.395E+01	6.991E+01	2.292E+02	4.035E+02	2.310E−03	7.051E+02
Sc^{13+}	3.946E−02	1.022E−01	3.977E−01	2.850E+00	2.089E+01	7.325E+01	2.494E+02	4.547E+02	3.030E−03	8.068E+02
Ti^{14+}	1.976E−01	7.588E−01	2.587E+00	1.166E+01	3.713E+01	8.169E+01	2.752E+02	5.092E+02	3.540E−03	9.705E+02
V^{15+}	2.565E−01	9.888E−01	3.415E+00	8.790E+00	3.525E+01	8.617E+01	3.009E+02	5.666E+02	4.340E−03	1.051E+03
Cr^{16+}	2.047E−01	4.183E−01	1.685E+00	4.760E+00	3.402E+01	9.074E+01	3.248E+02	6.257E+02	5.740E−03	1.272E+03
Mn^{17+}	8.408E−02	1.932E−01	1.204E+00	4.577E+00	3.063E+01	9.405E+01	3.509E+02	6.884E+02	6.010E−03	1.319E+03
Fe^{18+}	5.270E−03	1.510E−02	4.569E−01	2.863E+00	5.296E+01	1.059E+02	3.777E+02	7.527E+02	1.011E−02	1.719E+03
Co^{19+}	5.337E−02	2.040E−01	8.816E−01	2.148E+00	1.195E+01	8.936E+01	4.062E+02	8.207E+02	9.600E−03	1.747E+03
Ni^{20+}	7.610E−02	3.154E−01	1.751E+00	1.251E+01	5.188E+01	1.170E+02	4.352E+02	8.908E+02	1.195E−02	2.029E+03
Cu^{21+}	6.102E−02	2.490E−01	2.514E+00	1.386E+01	5.125E+01	1.229E+02	4.640E+02	9.593E+02	1.162E−02	2.016E+03
Zn^{22+}	1.502E−02	7.224E−02	2.635E+00	1.166E+01	4.893E+01	1.278E+02	4.952E+02	1.033E+03	1.405E−02	2.300E+03
Kr^{28+}	1.756E−01	1.538E+00	1.037E+01	6.020E+01	1.373E+02	2.013E+02	7.014E+02	1.528E+03	2.911E−02	3.952E+03
Mo^{34+}	8.268E−01	5.598E+00	2.100E+01	8.243E+01	2.420E+02	2.944E+02	9.469E+02	2.122E+03	4.689E−02	5.728E+03
Cd^{40+}	2.603E−01	5.110E−01	1.188E+01	8.850E+01	2.419E+02	3.787E+02	1.240E+03	2.820E+03	7.396E−02	7.950E+03
Xe^{46+}	1.252E−01	5.607E+00	1.837E+01	1.905E+02	4.956E+02	5.628E+02	1.613E+03	3.626E+03	1.112E−01	1.075E+04

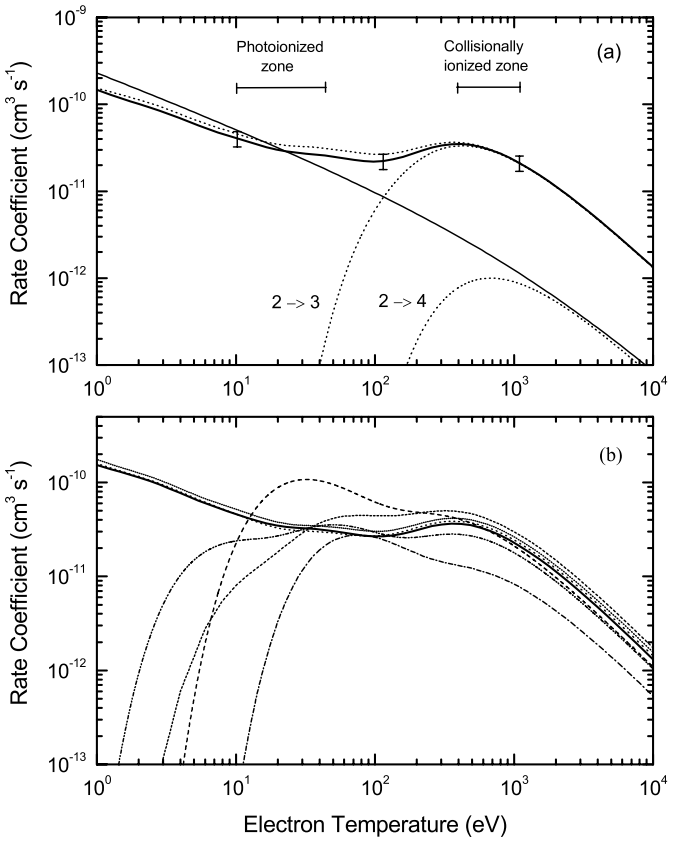

Fig. 2. Total DR Maxwellian rate coefficients for Fe^{18+} forming Fe^{17+} as a function of electron temperature (in eV). **a)** The *thick solid curve* represents the experimentally derived total DR rate coefficients, the error bars show the estimated experimental uncertainty of ≈20%. The *dotted curve* represents our MCBP calculations. Also shown are the contributions due to just the $2 \rightarrow 3$ and $2 \rightarrow 4$ core excitations. As a reference we also give the RR rate coefficients (*thin solid curve*). The temperatures of formation of Fe^{18+} in a photoionized plasma (Kallman & Bautista 2001) and in a collisionally ionized plasma (Mazzotta et al. 1998) are also shown. **b)** Comparison of our results (*thick solid curve*) with the theoretical total DR rate coefficients of Jacobs et al. (1977), as fitted by Shull & van Steenberg (1982, *dot-dashed curve*), the data of Roszman (1987, *dot-dot-dashed curve*), the results of Dasgupta & Whitney (1994, *short dashed curve*), as well as recommended total DR rate coefficients of Mazzotta et al. (1998, *dashed curve*), based on the HF calculations of Dasgupta & Whitney (1994). Also shown are the latest MCDF results from Savin et al. (2002, *coarsely dotted curve*) and the latest FAC results of Gu (2003b, *finely dotted curve*).

comes from the $2 \rightarrow 3$ core excitation. We also explored the contribution of the $2 \rightarrow 4$ core excitation. This process gives less than a 4% contribution to the total DR at higher temperatures ($kT \gtrsim 800$ eV), and hence we did not include it in our calculations for other ions of the sequence. As seen from Fig. 2b, there is a large disagreement with previous calculations of total DR for Fe^{18+}. These calculations do not include DR contributions due to $2 \rightarrow 2$ $\Delta l = 0$ fine-structure core transitions shown in Eq. (1). Thus, they do not reproduce the correct low-temperature behavior for the total DR rate coefficients, which, as mentioned above, are very important for modelling photoionized plasmas. At larger temperatures, there is also noticeable disagreement.

The total DR rate coefficient of Jacobs et al. (1977) is a factor of ≈3 smaller, and the results of Roszman (1987) are a factor of 1.2 smaller, than our data at the high-temperature peak in the total DR rate coefficients. Better agreement for higher temperatures is seen with the recommended total DR rate coefficients of Mazzotta et al. (1998), based on the HF calculations of Dasgupta & Whitney (1994), but these results significantly disagree with our results at lower temperatures. Approximately the same order of disagreement was found between our other total DR rate coefficients and that of the other oxygen-like ions presented in the above-mentioned works.

Excellent agreement was found with the latest MCDF results from Savin et al. (2002); these calculations differ from ours by using Dirac-Fock wave functions for the target description. Further MCDF calculations have been carried out by Chen (2002) for four members of the oxygen-like sequence: Mg^{4+}, Si^{6+}, S^{8+}, and Fe^{18+}. Those calculations also included the important configurations and spin–orbit effects as were included in our calculations, and indeed we find excellent agreement between those reported total DR rate coefficients and ours, further validating the improved accuracy of our results for the entire sequence up to Zn. Excellent agreement was also found with the FAC results for oxygen-like Mg, Si, S, Ar, Ca, Fe, and Ni of Gu (2003a,b) for the temperatures $T \geq 0.1$ eV at which those results were stated to be reliable. The FAC method is quite similar to our MCBP method.

Our calculations have been carried out in the independent processes approximation, i.e., we neglect interference between the RR and DR pathways. It has been shown (Pindzola et al. 1992; Gorczyca et al. 1996) that interference effects have generally only a very small effect on the total (and strongest partial) rate coefficients. Furthermore, even when noticeable asymmetric interference profiles *can* be observed, their effect is negated once the energy-integrated rates are computed.

In order to further investigate interference effects for the case of DR of oxygen-like ions, we also performed R-matrix calculations for $2s \rightarrow 2p$ DR on F^+ and Ne^{2+}. Figure 3a compares the Ne^{2+} DR cross sections obtained with our radiation-damped R-matrix code (Robicheaux et al. 1995; Gorczyca et al. 1995) and the AUTOSTRUCTURE code. We see very close agreement in the cross sections, summed-over all final states, except for a few small differences in the threshold peak (a similar comparison was obtained for F^+).

It is instructive to break up the partial DR cross section into three radiative contributions (Fig. 3b):

$$e^- + Ne^{2+}(2s^2 2p^4) \rightarrow$$

$$Ne^+(2s2p^5 nl) \rightarrow Ne^+(2s^2 2p^5) + h\nu \quad \text{ground state decay}, \quad (5)$$

$$\rightarrow Ne^+(2s2p^5 nl) + h\nu \quad \text{valence decay}, \quad (6)$$

$$\rightarrow Ne^+(2s^2 2p^4 nl) + h\nu \quad \text{core decay}. \quad (7)$$

The only interference effects, on this scale, are seen in the ground state decay, which is the inverse of photoionization from the Ne^+ ground state, as dips below the background cross section. However, the ground state decay process contributes an insignificant amount to the total cross section compared to the other channels, especially the core decay channels. The core decay channels show no noticeable interference because the

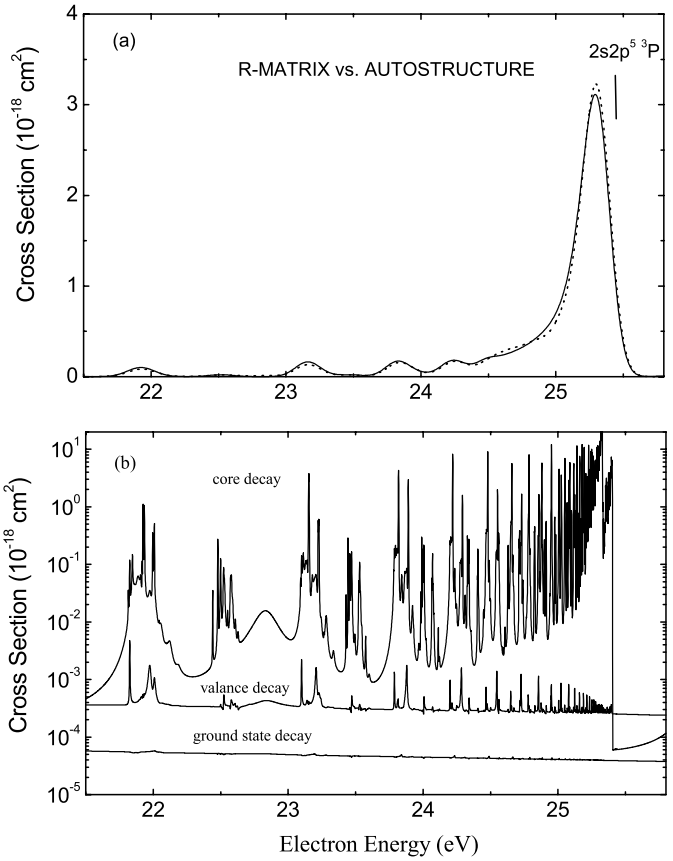

Fig. 3. DR cross sections for Ne^{2+} for 2s → 2p core excitation. **a)** Comparison of cross sections obtained with R-matrix (*solid curve*) and AUTOSTRUCTURE (*dotted curve*) codes. The cross sections were convoluted with a Gaussian electron distribution of 0.1 eV FWFM. **b)** Contribution of different decay modes to the total DR cross section. The region below 21 eV is devoid of resonances formed due to a 2s → 2p core excitation.

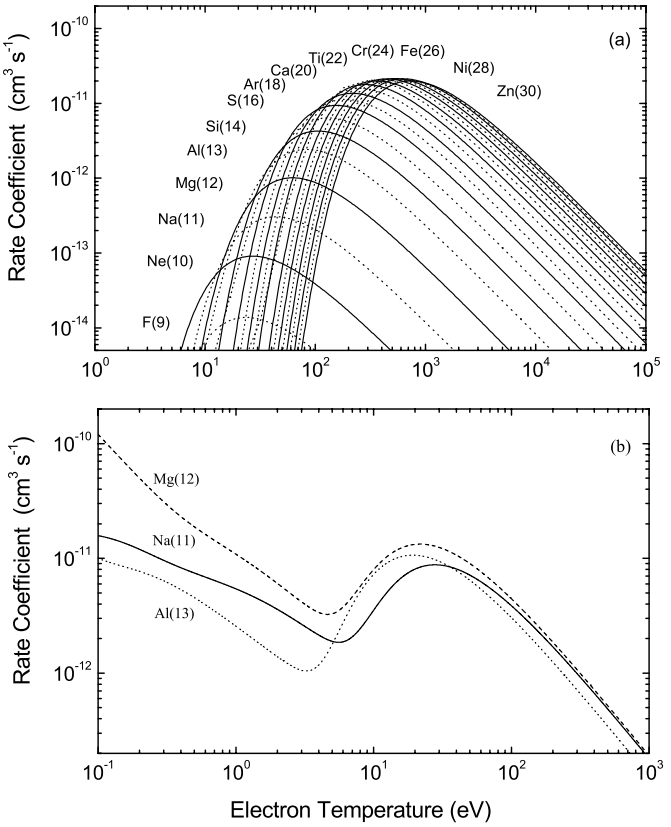

Fig. 4. Behavior of total DR rate coefficients. **a)** Total rate coefficients for the $\Delta n_c = 1$ DR for O-like F through Zn as a function of their atomic number (given in parenthesis). Not all ions are labelled. **b)** Total rate coefficients for the $\Delta n_c = 0$ DR for Na^{3+}, Mg^{4+}, and Al^{5+} showing irregular dependence on Z.

direct $\varepsilon l \rightarrow nl$ RR decay is much smaller the resonant DR. It is well known that *photoionization* cross sections show large asymmetric interference profiles, and this may be the root of the incorrectly held opinion that interference effects are important in DR. This notion is false because those decay routes which do show interference contribute insignificantly to the *total* cross section. We note that the difference between the AUTOSTRUCTURE and the R-matrix total DR rate coefficient for F^+ and Ne^{2+} is less than 1%, indicating that interference effects are negligible in the rate coefficients. However, the R-matrix calculations took ≈100 times longer to perform than the AUTOSTRUCTURE ones. Furthermore, Pindzola et al. (1992) examined the effect of interference on partial recombination cross sections. They found that, on averaging over the resonance profile, the effect of interference was severely reduced and only significant for certain weak resonances.

In Table 1, we present the fitting parameters for total DR rate coefficients for each ion from F^+ to Zn^{22+}. In previous works, numerical calculations have been performed only for some ions in the sequence and the total DR rate coefficients for other ions are interpolated (or extrapolated) assuming smooth behavior of total DR rate coefficients as a function of nuclear charge. For example, Roszman (1987) obtained numerical results for Ar^{10+}, Fe^{18+}, Kr^{28+}, and Mo^{34+} ions, and these results were used to derive an analytic interpolation formula for the whole oxygen-like sequence. Similarly, Dasgupta & Whitney (1994) presented scaling relations, which can be used for any ion with atomic number $18 \leq Z \leq 34$ and which were obtained on the basis of numerical results for Ar, Ti, Fe, and Se ions. However, we have found that such analytic interpolation formula are only applicable for the 2 → 3 DR rate coefficients (Fig. 4a), because our 2 → 2 DR rate coefficients behave rather irregularly at lower temperatures, not acting smoothly as a function of Z, as seen in Fig. 4b. The irregular behavior of the 2 → 2 DR rate coefficients is explained by the fact that autoionizing levels that are just above threshold for one value of Z move just below threshold for a neighboring $Z+1$ member of the series, becoming a bound state and not contributing to DR. For example, the $2s2p^5nl$ ($n = 4, 5$) levels in the low-charged ions F^+ and Ne^{2+} are autoionizing, whereas in Fe^{18+} they are all bound. Such a drastic change in the number of near-threshold autoionization levels is the reason for irregular behavior of the total DR rate coefficients at low temperatures.

Another reason for the discrepancy with earlier calculations is that most of those were performed in LS-coupling neglecting

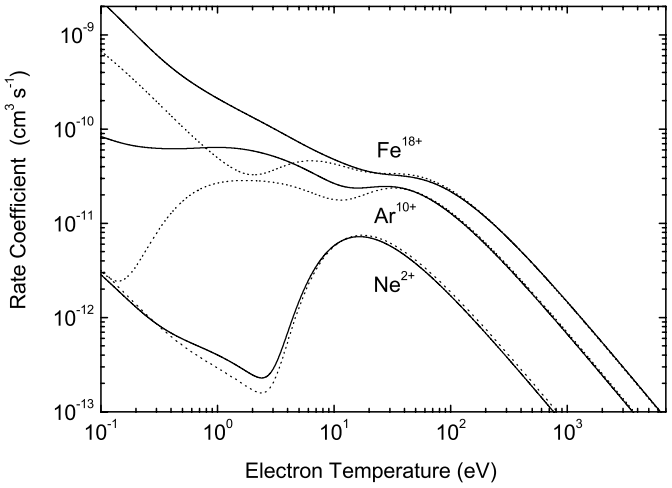

Fig. 5. Comparison of our $2 \rightarrow 2$ DR rate coefficients obtained in LS-coupling (*dotted curves*) and in intermediate-coupling (*solid curves*).

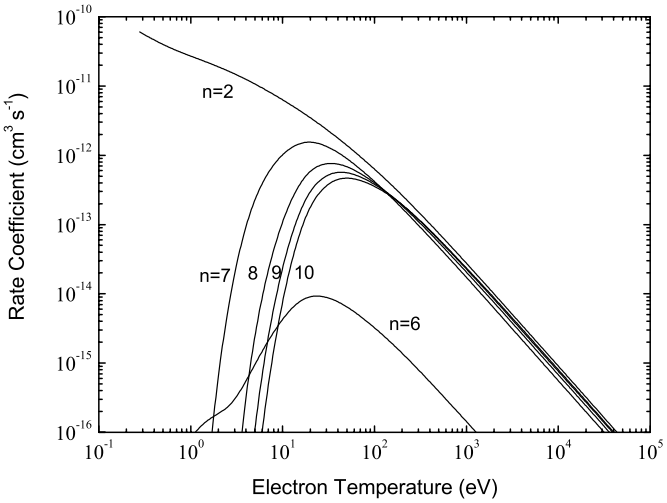

Fig. 6. DR final-state resolved rate coefficients for Fe^{18+} as a function of electron temperature. We present the DR final-state resolved rate coefficients from the initial $2p^4\ ^3P_2$ level to the final $2p^4nl$ states with given n.

spin-orbit effects. This approximation can lead to considerable error in the total DR rate coefficients. Comparison of our LS and IC results for some oxygen-like ions with different nuclear number are given in Fig. 5. We see rather large differences between the LS and IC results at low temperatures. The smaller values for the LS total DR rate coefficients at small temperatures can be explained by the fact that in LS-coupling, the autoionizing $2s^22p^4(^3P_{0,1,2})nl$ states in Eq. (1) are not included.

In addition to the total DR rate coefficients, the *adf09* files also contain information about the population from DR of the resolved final states, which is required for collisional–radiative modelling of dense plasmas. As an example of the final state-resolved rate coefficients available, we present in Fig. 6 the Fe^{18+} $2 \rightarrow 2$ DR rate coefficients for population of final $2p^4nl$ states with different n-values (the processes depicted in the first line of Eq. (1)). We see that at low temperatures, as expected, the ion preferentially recombines into the ground $2p^5\ ^2P$ level ($n = 2$) due to its lower energy. The population of the excited $2p^4nl$ levels smoothly decreases with increasing temperature. The absence of noticeable populations of the $2p^4nl$ states with $2 < n < 6$ can be explained by the fact that the $2s2p^5nl$ levels with $n < 6$ in Fe^{18+} are bound states, and the small population of the $2p^46l$ state is because the only some of the $2s2p^46l$ levels are bound. Of course, there exists hundreds of final levels for this ion alone, for which the DR final level-resolved rate coefficients are tabulated in the *adf09* files. Here, we only plot a few examples as an illustration of the available data.

In general, DR from initial metastable states is also required for collisional-radiative modelling of dynamic plasmas. The reason for this is that significant populations can build up in the metastables and they are not necessarily in quasi-static equilibrium with the ground state. Figure 7 presents examples of DR rate coefficients from the initial ground and metastable states $2p^4\ ^3P$, ^1D and ^1S in an LS-coupling approximation. We see that the rate coefficients for different initial terms are quite different at small temperatures. This can be explained by the different contributions from each process indicated in Eq. (1). As in the case of the total rate coefficients from the ground

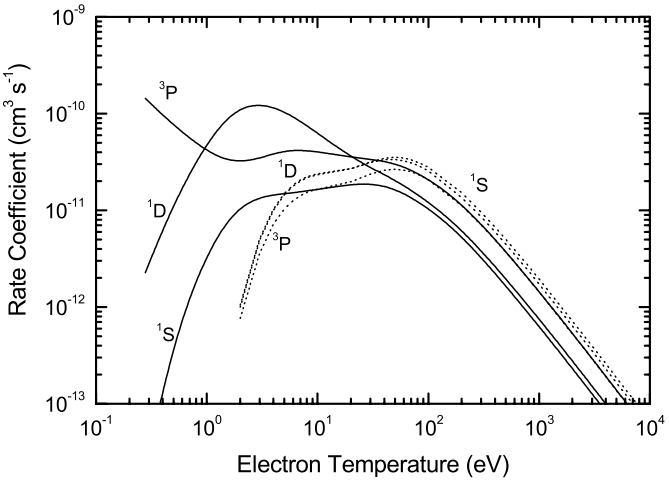

Fig. 7. DR initial-state resolved LS-coupling rate coefficients for Fe^{18+} as a function of electron temperature (*solid curves*) compared with the results of Roszman (1987, *dotted curves*). We present DR rate coefficients for the $2p^4\ ^3P$,^{1} D, and ^{1}S initial metastable states.

state, Fig. 2, here we also see large discrepancies with previous calculations of Roszman (1987). This is due to the fact that Roszman used the average-configuration approximation, in which all terms of the $2p^4$ configuration have the same energy. A more detailed study of DR from metastable levels has been carried out by Chen (2002) using MCDF techniques.

4. Summary

In this paper, we have systematically calculated partial and total DR rate coefficients along the oxygen-like sequence as part of an assembly of a DR database necessary for the modelling of dynamic finite-density plasmas (Badnell et al. 2003). The approximations used for generating our data have been

recently validated by the good agreement of DR resonance strengths and energies between our theoretical data and the experimental results from the Test Storage Ring in Heidelberg for highly-charged Fe^{18+} (Savin et al. 1999, 2002a). To assess the reliability of our calculations for the low-charged end of this isoelectronic sequence, we compared between theoretical R-matrix and perturbative results. All calculations have been made in intermediate-coupling, so that fine-structure effects are incorporated. Both $2 \rightarrow 2$ and $2 \rightarrow 3$ core excitations have been included in order to span a wide temperature range. We have presented selected initial and final state-resolved and total rate coefficients for some ions of interest and have made comparisons, where possible, with previous work. We found large disagreement with previous calculations, including the recommended DR data of Mazzotta et al. (1998) which were used in their study of the ionization equilibrium for different atoms. Final-state-resolved DR rate coefficients have been tabulated, and these data are available from the web site `http://www-cfadc.phy.ornl.gov/data_and_codes`. Total DR and RR rate coefficients have been fitted by simple analytic formulae, which will also prove of great use to astrophysical and fusion plasma modellers, and are available on our web site `http://homepages.wmich.edu/~gorczyca/drdata`.

We have calculated our data over a wide temperature range and for a large number of atomic ions in order to maximize the available information for modelling work. Our fits are accurate to better than 3% for all ions in the wide temperature range from $\approx 10^1$ to 10^8 K. The main source of uncertainty in our computed rate coefficients is due to the uncertainty in resonance positions near threshold. However, this only affects a temperature range much lower than the photoionized and collisionally ionized zones of interest. These RR and DR data are suitable for modelling of solar and cosmic plasmas under conditions of collisional ionization equilibrium, photoionization equilibrium, and non-equilibrium ionization (e.g. in shocks). In the future, we will present DR data for further isoelectronic sequences as detailed previously (Badnell et al. 2003).

Acknowledgements. T.W.G., K.T.K., and O.Z. were supported in part by NASA Space Astrophysical Research and Analysis Program grant NAG5-10448. D. W. S. was supported in part by NASA Space Astrophysics Research and Analysis Program grant NAG5-5261 and NASA Solar Physics Research, Analysis, and Suborbital Program grant NAG5-9581.

References

Badnell, N. R. 1986, J. Phys. B, 19, 3827
Badnell, N. R., & Pindzola, M. S. 1989, Phys. Rev. A, 39, 1685
Badnell, N. R. 1997, J. Phys. B, 30, 1
Badnell, N. R., O'Mullane, M. G., Summers, H. P., et al. 2003, A&A, 406, 1151 (Paper I of this series)
Berrington, K. A., Eissner, W. B., & Norrington, P. H., 1995, Comput. Phys. Commun., 92, 290
Chen, M. H. 2002, Phys. Rev. A, 66, 052715
Cowan, R. D. 1981, The Theory of Atomic Structure and Spectra (Berkeley: University California Press)
Dasgupta, A., & Whitney, K. G. 1994, At. Nucl. Data Tables, 58, 77
Dasgupta, A., & Whitney, K. G. 1995, J. Phys. B, 28, 515
Froese Fisher, C. 1991, Comput. Phys. Commun., 64, 369
Gorczyca, T. W., Robicheaux, F., Pindzola, M. S., & Badnell, N. R. 1995, Phys. Rev. A, 52, 3852
Gorczyca, T. W., Robicheaux, F., Pindzola, M. S., & Badnell, N. R. 1996, Phys. Rev. A, 54, 2107
Gorczyca, T. W., Badnell, N. R., & Savin, D. W. 2002, Phys. Rev. A, 65, 062707
Gu, M. F. 2003a, ApJ, 582, 1241
Gu, M. F. 2003b, ApJ, 590, 1131
Jacobs, V. L., Davis., J., Kepple, P. C., & Bhala, M. 1977, ApJ, 211, 605
Jacobs, V. L., Davis., J., Kepple, P. C., & Bhala, M. 1977, ApJ, 215, 690
Jacobs, V. L., Davis, J., Kepple, P. C., & Bhala, M. 1979, ApJ, 230, 627
Jacobs, V. L., Davis, J., Rogerson, J. E., et al. 1980, ApJ, 239, 1119
Kallman, T. R., & Bautista, M. 2001, ApJS, 133, 221
Mazzotta, P., Mazzitelli, G., Colafrancesco, S., & Vittorio, N. 1998, A&AS, 133, 403
Robicheaux, F., Gorczyca, T. W., Pindzola, M. S., & Badnell, N. R. 1995, Phys. Rev. A, 52, 1319
Roszman, L. J. 1987, Phys. Rev. A, 35, 3368
Pindzola, M. S., Badnell, N. R., & Griffin, D. C. 1992, Phys. Rev. A, 46, 5725
Ramirez, J. M., & Bautista, M. 2002, J. Phys. B, 35, 4139
Savin, D. W., Kahn, S. M., Linkemann, J., et al. 1999, ApJS, 123, 687
Savin, D. W., & Laming, J. M. 2002, ApJ, 566, 1166
Savin, D. W., Kahn, S. M., Linkemann, J., et al. 2002a, ApJ, 576, 1098
Savin, D. W., Behar, E., Kahn, S. M., et al. 2002b, ApJS, 138, 337
Schippers, S., Müller, A., Gwinner, G., et al. 2001, ApJ, 555, 1027
Seaton, M. J. 1969, J. Phys. B, 2, 5
Shull, J. M., & van Steenberg, M. 1982, ApJS, 46, 95
Summers, H. P. 1999, ADAS User Manual (2nd ed.), available from `http://adas.phys.strath.ac.uk/adas/docs/manual`
Verner, D. A., & Ferland, G. J. 1996, ApJS, 103, 467